Tellus (2003), 55B, 808–819
Printed in UK. All rights reserved

TELLUS
ISSN 0280–6509

Simultaneous dry and ambient measurements of aerosol size distributions at the Jungfraujoch

By R. NESSLER[1,2], N. BUKOWIECKI[1], S. HENNING[1], E. WEINGARTNER[1,*], B. CALPINI[3] and U. BALTENSPERGER[1], [1]*Laboratory of Atmospheric Chemistry, Paul Scherrer Institut (PSI), CH-5232 Villigen PSI, Switzerland;* [2]*Laboratory for Air and Soil Pollution (LPAS), Swiss Federal Institute of Technology, CH-1015 Lausanne, Switzerland;* [3]*MétéoSuisse, Aerological Station Payerne, CH-1530 Payerne, Switzerland*

(Manuscript received 2 May 2002; in final form 27 January 2003)

ABSTRACT

In a field campaign at the high-alpine site Jungfraujoch (JFJ, 3580 m asl), in-situ aerosol size distributions were measured simultaneously outdoor at ambient conditions (temperature $T < -5$ °C) and indoor at dry conditions ($T \approx 25$ °C and relative humidity RH $< 10\%$) by means of two scanning mobility particle sizers (SMPS). In addition, measurements of hygroscopic growth factors were performed with a hygroscopicity tandem differential mobility analyzer (H-TDMA). The measured growth factors, being a monotonic function of the relative humidity (RH), were fitted with a modified Köhler model. A comparison between dry and ambient size distributions shows two main features: First, the dry total number concentration is often considerably smaller (on average 28%) than the ambient total number concentration, and is most likely due to the evaporation of volatile material at the higher temperature. These particle losses mainly concern small particles (dry diameter $D \lesssim 100$ nm), and therefore have only a minimal affect on the surface and volume concentrations. A slight correlation between ambient RH and the magnitude of particle loss was observed, but it was not possible to establish an empirical model for a quantification. Second, the dry number size distribution is shifted towards smaller particles, reflecting the hygroscopic behavior of the aerosols. To link the ambient and the dry size distributions we modeled this shift using the H-TDMA measurements and a modified Köhler model. The corrected dry surface and volume concentrations are in good agreement with the ambient measurements for the whole RH range, but the correction works best for RH $< 80\%$. The results indicate that size distribution data measured at indoor conditions (i.e. dry and warm) may be successfully corrected to reflect ambient conditions, which are relevant for determining the impact of aerosol on climate.

1. Introduction

The size of aerosol particles is of crucial importance to several processes in the atmosphere. Particles with diameters in the range $0.1 < D < 1$ μm are highly effective at scattering and, depending on their chemical composition, at absorbing incoming solar radiation. These processes are known as the direct aerosol effect. In addition, water-soluble particles with $D \gtrsim 100$ nm may act as cloud condensation nuclei (CCN) and contribute to the indirect effect. The direct effect can result in a positive or negative radiative forcing, depending on the chemical composition of the aerosols. The indirect effect is thought to result in a negative global mean radiative forcing, which may be negating the positive forcing due to greenhouse gases. The uncertainty is still largely due to the poorly quantified influence of tropospheric aerosols on climate (IPCC, 2001; Ramanathan et al., 2001).

The Jungfraujoch High Alpine Research Station (JFJ) is located at an altitude of 3580 m and is most often above the convective boundary layer. Consequently, the site is not affected by regional pollution sources. This makes the JFJ an ideal site for the long-term observation of climate-relevant aerosol

*Corresponding author.
e-mail: ernest.weingartner@psi.ch

parameters in the free troposphere, which is one of the goals of the World Meteorological Organization's (WMO) Global Atmosphere Watch (GAW) program (Nyeki et al., 1998). This program was established to provide measurements, scientific assessments, and other information on changes in the global chemical composition and related physical characteristics of the atmosphere. Concerning aerosols, the objective of the GAW program is to determine the spatio-temporal distribution of aerosol properties related to climate forcing and air quality up to multi-decadal time scales (WMO, 2001).

Unfortunately, aerosol in-situ measurements suffer from the inconvenience that they usually have to be performed by inducting the ambient air into a housing, and therefore, are sampled at a different temperature (T) and relative humidity (RH). Thus, the measured aerosol properties may differ from the ambient (the climate-relevant) ones. This is particularly true at places exposed to such extreme meteorological conditions as the JFJ with average temperatures of $-1\,^{\circ}$C in summer and $-14\,^{\circ}$C in winter and an average annual relative humidity of 74%. Since the laboratory and the instrumentation is kept at a much higher temperature (at 20–30 $^{\circ}$C) relative to the ambient conditions, the RH of the sampled aerosol typically drops to less than 10%.

To investigate the bias introduced by this change in temperature and RH, an extensive field campaign at the JFJ was conducted, and for the first time in-situ aerosol size distribution measurements were performed outdoors at such extreme ambient conditions by means of a scanning mobility particle sizer (SMPS). Simultaneously, the size distributions were measured conventionally in the laboratory. To simplify the terminology, these indoor measurements are henceforth referred to as dry measurements, in contrast to the ambient measurements performed outdoors. The terms ambient and dry will also be used for size distributions and concentrations. In addition, hygroscopic growth factors were measured with a hygroscopicity tandem differential mobility analyzer (H-TDMA).

The objective of this paper is to report the results of the described measurements and to present a method to link the ambient and the dry size distributions, which allows for a better understanding of the aerosol properties relevant for the direct climatic effect. In this study no cloud activation mechanisms were explored. Consequently, this work does not focus on the indirect climatic effect of aerosols. An investigation of humidity effects on optical aerosol properties can be found in Bundke et al. (2002).

2. Experimental

From 2 February to 31 March 2000 the Cloud and Aerosol Characterization Experiment (CLACE) was performed at the JFJ research station with the participation of eight Swiss, German, and Hungarian research groups. Extensive measurements of aerosol microphysical and optical properties, volatility and chemical composition were performed. Additional results to those presented here are reported in Weingartner et al. (2002) and Henning et al. (2002). The synthesis of the CLACE dataset with lidar measurements performed at the same time on the JFJ by the EPFL lidar group will be addressed in a future paper.

Aerosol particles were sampled from an interstitial inlet, which was designed to remove all cloud droplets at an early stage in the sampling process. This inlet consisted of the upper four stages of a small deposit area cascade impactor (SDI, Maenhaut et al., 1996) which generated a final cut-off of $D = 1\ \mu$m at a flow rate of 11 L min^{-1}. Great care was taken that the impactor was operated at ambient temperature such that the supercooled cloud droplets were immediately removed by contact freezing at the corresponding impactor stage. The functioning of this method was tested under controlled conditions in the laboratory (Tenberken-Pötzsch et al., 2000) as well as in the field (Henning et al., 2002). In order to prevent a clogging of the impactor, sampling was interrupted once a day and the inlet was replaced with a cleaned and dried impactor.

Behind the inlet, the flow was split for the H-TDMA, the ambient and the dry SMPS (see below), and a flow controller generating a total flow of 11 L min^{-1} (Fig. 1). For the determination of the hygroscopic growth factors D/D_{dry} (defined as the ratio of the humidified particle diameter D to the dry particle diameter D_{dry}) the aerosol was first dried with a silica gel diffusion dryer (to RH $\approx$ 10%) and then fed into the low-temperature H-TDMA (Weingartner et al., 2002). The H-TDMA was submersed in a water/ethylene glycol bath and kept at a constant temperature of $-10\,^{\circ}$C, which was close to ambient (outdoor) temperature. In this instrument a narrow size range of the polydisperse dry aerosol is selected with a first differential mobility analyzer (DMA). This monodisperse aerosol is then humidified, and the resulting size of the wet particles

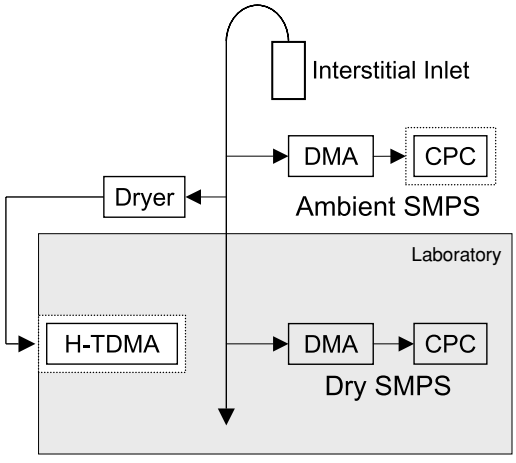

Fig. 1. Sketch of outdoor (at ambient RH and T) and indoor (at RH $< 10\%$ and $T = 20$–$30\ ^{\circ}$C) measurements.

is measured with a second DMA and a condensation particle counter (CPC). Although the drying process may cause volatilization losses of components other than water, great care was taken to minimize these losses and to maintain the original aerosol composition as far as possible. Therefore, the diffusion dryer as well as the tubing to the entrance of the H-TDMA were kept at ambient temperature.

Ambient and dry size distributions were measured with two identical SMPS systems that consisted of a bipolar charger to obtain charge equilibrium (krypton source, ^{85}Kr), a DMA (TSI 3071) and an CPC (TSI 3022A). The poly- and monodisperse flows were 0.3 L min^{-1}, while sheath and excess air flows were 3 L min^{-1}. The sheath and excess flows were operated in a closed-loop system and were held constant by a critical orifice. Apart from the stability of this configuration, the same gas composition was ensured both inside the DMA and in the sampled air, therefore minimizing any possible sampling artifacts. Flows were calibrated periodically with a bubble flowmeter to $\pm 1\%$. With this setup the aerosol size distributions from $D = 18$ to 800 nm were measured at an average ambient pressure of 650 hPa. The high voltage of the ambient SMPS was further restricted to 6.5 kV to prevent electrostatic breakdown, resulting in an upper size limit of 634 nm. Scanning of the DMA voltage was performed in logarithmically equidistant steps with a time resolution of about 6 min per scan (300 s up scan time, 10 s down scan and 60 s wait time resulting in a scanning velocity of $\mathrm{d}\log D/\mathrm{d}t = 5.7 \times 10^{-3}$ s^{-1}). With this scanning velocity no deformation of the size distribution occurs (Weingartner et al., 2002).

For the measurement of the ambient size distribution, a "naked" DMA column was mounted at the well ventilated railing of the sphinx building, and the HV connector was modified to allow such an "unprotected" operation. A heat exchanger was used to allow the warmer sheath air exiting the pump to equilibrate to ambient temperature. This configuration allowed for the measurement of the size distribution under ambient conditions, i.e. at ambient temperature and RH. Due to the closed-loop system changes in the ambient RH were slightly delayed in the ambient SMPS. Weingartner et al. (2002) investigated the RH transfer inside an H-TDMA with the same sheath air configuration as the ambient SMPS used in this study. An abrupt RH change occurring at the inlet to the closed-loop system will result in a 50% equilibration of the RH after 7 min and a 90% equilibration after 18 min. One-hour averages (see below) of ambient RH are therefore appropriate to characterize RH inside the ambient SMPS. The ambient CPC was located in an insulated box which was heated to a controlled temperature of 10 °C. Thermal insulation was necessary to protect this instrument from the harsh weather conditions and to insure proper functioning of the CPC. The tube length from the exit of the DMA to the CPC entrance was ≈30 cm and contributed less than 1 s to the delay time of an SMPS scan. It is assumed that there are negligible changes in the number concentration due to particle evaporation during this short transfer time. For the measurement of the dry size distribution, the interstitial aerosol was fed into the building (indoor $T = 20$–$30\ ^{\circ}$C, RH $< 10\%$) and was sampled with another SMPS system. This system was operated in an identical manner as the ambient SMPS. Summarizing, the ambient SMPS worked at wet and cold conditions, the dry SMPS at dry and warm conditions. The H-TDMA measured the uptake of water by the particles at different RH under cold conditions. The possible losses of volatile constituents within the H-TDMA dryer are not known; therefore, the possible contribution of these species to the hygroscopic growth of the aerosol has been neglected.

The presence of clouds was determined by measuring the cloud liquid water content (LWC) with a particle volume monitor (PVM-100, Gerber Scientific Inc, USA), and the threshold for cloud presence was set at a LWC = 0.02 g m^{-3}. The cloud measurement setup is described in detail in Henning et al. (2002). In addition, continuous meteorological

measurements (wind direction, wind velocity, air pressure, air temperature, relative humidity and solar radiation) were obtained from the Swiss Meteorological Institute (MeteoSwiss). For further data processing 1-h averages of SMPS and meteorological data were calculated. All shown size distributions are smoothed by 5-bin gliding window averaging. The bin size used is the constant log-diameter interval 0.015, i.e. $\log(D_{i+1}) - \log(D_i) = 0.015$.

3. Results

3.1. H-TDMA measurements

Detailed results of the H-TDMA measurements are reported in Weingartner et al. (2002). Here only a synopsis of the most important features is given. During the CLACE campaign, the hygroscopic growth of particles with dry diameters $D_{\mathrm{dry}} = 50, 100$ and 250 nm was measured continuously at a constant RH of 85% in the second DMA. Most of the time, the station was located in the free troposphere, and the shape of the H-TDMA size spectra was primarily characterized by a narrow monomodal growth distribution (only ≈7% of the particles experienced a smaller hygroscopic growth than the particles in the dominant mode). This implies that the particles in the observed size range were to a large extent internally mixed. Exceptions from this behavior were limited to short time periods when the station was influenced by local pollution due to construction work or dust plumes from North Africa (Saharan dust). The presence of dust produced bimodal growth distributions consisting of a more hygroscopic mode and a less hygroscopic mode.

During several episodes the RH in the second DMA was varied to study the RH dependence of the hygroscopic growth. Figure 2 (circles) shows two such events (6 March and 16 March 2000) when the station was clearly located in the FT. No distinct deliquescence behavior was observed, and this is explained by the multicomponent chemical composition of the particles (cf. section 3.2). The data were acquired with a time resolution of 5 min. After three scans (i.e. after 15 min) the applied voltage of the first DMA was changed such that $D_{\mathrm{dry}} = 50$, 100 and 250 nm particles were measured alternately with a high resolution. The acquisition of all points in Fig. 2 with 20% < RH < 80% required 6 h for two sweeps of the RH range.

The solid lines are fitted growth curves, based on the modified Köhler equation (cf. equation (A1) in the Appendix) introduced by Brechtel and Kreidenweis (2000). These curves can be used to interpolate and extrapolate the hygroscopic growth of the particles. The two unknown fit parameters Y_{f} and $\beta_{0,\mathrm{f}}$ were found to be $Y_{\mathrm{f}} = 39 \pm 4$, 40 ± 2 and 41 ± 5 kmol m^{-3} and $\beta_{0,\mathrm{f}} = (-0.1 \pm 0.1) \times 10^{-2}$, $(-0.5 \pm 0.8) \times 10^{-3}$ and $(-0.4 \pm 0.6) \times 10^{-3}$ kg mol^{-1} for the dry diameters 50, 100 and 250 nm, respectively.

Y_{f} and $\beta_{0,\mathrm{f}}$ depend on the chemical composition of the soluble fraction of the aerosol. Therefore, the

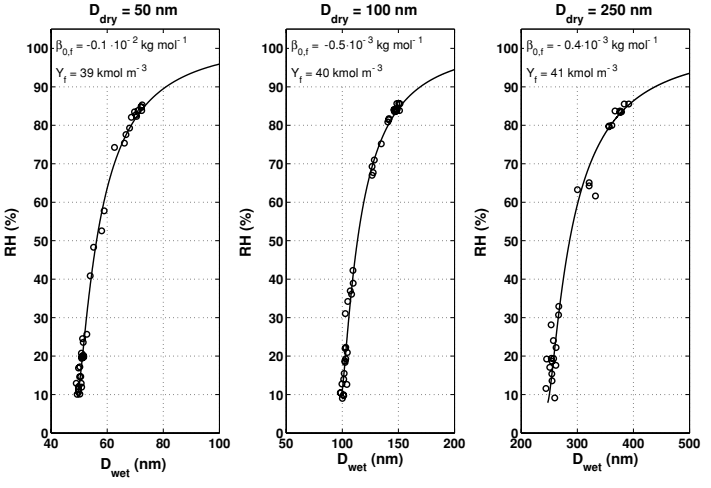

Fig. 2. Particle growth for dry diameters $D_{\mathrm{dry}} = 50$, 100 and 250 nm measured at the JFJ with the H-DTMA at $T = -10$ °C during RH scans (circles). The solid lines are fitted modified Köhler curves [cf. eq. (A1) in Appendix].

experimentally determined values for these two parameters allow some inference on the chemical composition of the analyzed aerosol. Noting that these values are essentially the same for dry diameters 50, 100 and 250 nm leads to the conclusion that the chemical composition also does not vary strongly in this diameter domain. Brechtel and Kreidenweis (2000) list calculated values of Y_f and $\beta_{0,f}$ for several solutes. The values we found accord best with those for ammonium nitrate (NH_4NO_3) and an equimolar mixture of ammonium sulfate and ammonium nitrate ($(NH_4)_2SO_4$-NH_4NO_3). Even though this result has to be handled with care, due to the complex chemistry of an ambient aerosol, it is very reasonable: Krivacsy et al. (2001) found that ammonium (NH_4), nitrate (NO_3) and sulfate (SO_4) are major components (typically about 70%) of the soluble part of the JFJ aerosol ($PM_{2.5}$), with the remainder being water-soluble organic compounds. Similar results are also reported in Henning et al. (2003).

3.2. SMPS measurements

A comparison of the dry and ambient SMPS measurements shows two main features: First, the dry size distribution is shifted towards smaller particles (cf. Figs. 3b and 3c). Second, the dry total number concentration is often considerably smaller (on average 28%) than the ambient total number concentration (cf. Figs. 3a and 3c).

The first feature reflects the hygroscopic behavior of aerosols: as shown in Fig. 2, the particle size is a monotonic function of RH, which allows for correction of the shift in the size distribution due to RH changes. This will be addressed in further detail in section 3.3.

Also for the second feature, the loss of particles in the dry distributions, the hygroscopicity has to be considered. Because of the hygroscopic shift towards smaller particles, the dry and the ambient SMPS do not detect particles in exactly the same dry diameter interval. Some particles at the lower end of the wet spectrum fall below the detection limit when dried, whereas some particles at the upper end of the dry spectrum grow beyond the detection limit when wet. Depending on the shape of the spectrum one or the other effect can prevail and cause an apparent net particle loss or gain in the dry SMPS. To investigate if the hygroscopic behavior of the particles is (at least partially) responsible for the found particle loss, we recalculated the total concentrations with slightly modified integration limits (c.f. Fig. 4). Instead of integrating both the dry and ambient distributions from D_1 to D_4, the dry distributions were integrated from D_1 to D_3 and the ambient distributions from D_2 to D_4. D_1 and D_4 correspond to the lower and upper detection limit of the SMPS systems, respectively. D_2 is equal

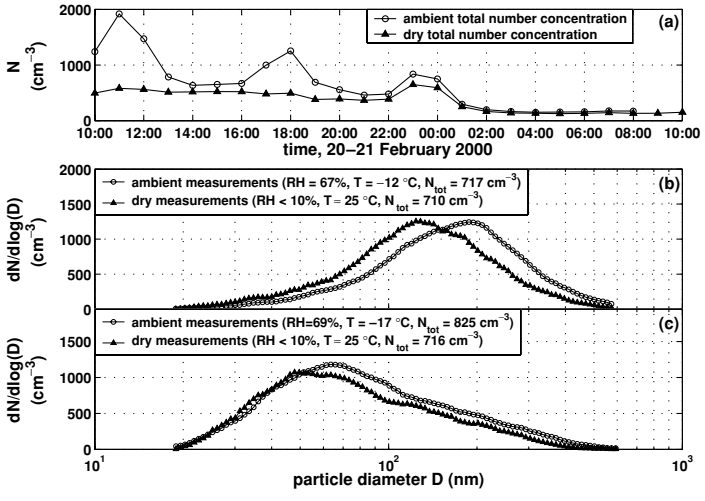

Fig. 3. One-day example of the comparison between ambient and dry total number concentration (1-h averages, integrated SMPS measurements) (a) as well as two snapshots, each showing a reduction in size for the dry number distribution, the first one without a reduction in the number concentration (b), the second one with a reduction in the number concentration (c). The number distributions are 5-bin gliding averages.

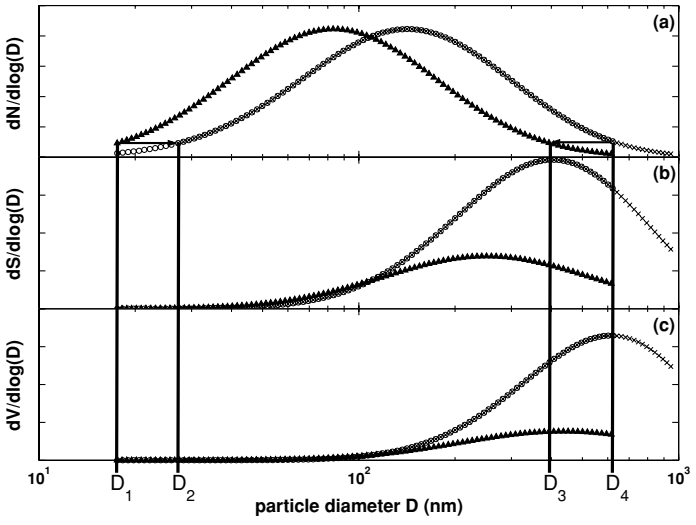

Fig. 4. Fictitious measurement of an ambient (circles) and a dry (triangles) distribution together with the corrected dry distribution (crosses) to illustrate the integration limits used for the calculation of the total concentrations: (a) number, (b) surface and (c) volume distribution. D_2 is equal to $G(D_1, \mathrm{RH})\ D_1$ and D_3 is given by $G(D_3, \mathrm{RH})D_3 = D_4$, where G(diameter, RH) is the hygroscopic growth factor for a given dry diameter and ambient RH.

to $G(D_1, \mathrm{RH})\ D_1$ and D_3 is given by $G(D_3, \mathrm{RH})\ D_3 = D_4$, where G(diameter, RH) is the hygroscopic growth factor for a given dry diameter and ambient RH. With these integration limits the ambient and dry total concentrations are integrated over the same dry diameter interval. The growth factors were individually calculated for each single spectrum according to the model presented in section 3.3. The adjusted total concentrations still show on average 28% fewer particles in the dry than in the ambient measurements. The fact that the loss does not change with the adjusted integration limits shows that the spectra fall towards zero within the detection limits of the SMPS systems for most of the cases (see also Fig. 3b). Therefore, the calculated particle loss is hardly sensitive to errors in the growth factors $G(D_1, \mathrm{RH})$ and $G(D_3, \mathrm{RH})$. However, the hygroscopic behavior of the aerosols cannot explain the particle loss. We hypothesize that the loss occurs due to the presence of volatile material, which evaporates during the drying process resulting in a diameter below the SMPS detection limit. In the case of ammonium nitrate, which is present in the Jungfraujoch aerosol (Henning et al., 2003), this evaporation is widely discussed in the literature (cf. e.g. Stelson and Seinfeld, 1982; Larson and Taylor, 1983; Mozurkewich, 1993). Stelson and Seinfeld (1982) examined the relative humidity and temperature dependence of the (pure) ammonium nitrate dissociation constant. They report that a temperature rise from 0 to 25 °C causes an increase of the dissociation constant of several orders of magnitude, resulting in the evaporation of the ammonium nitrate. As the outdoor temperature during CLACE never exceeded −5 °C, similar behavior can be expected. Indeed, Henning et al. (2003) report that all ammonium nitrate evaporated during sampling onto Teflon filters.

According to Stelson and Seinfeld (1982) pure ammonium nitrate at temperatures below 0 °C is solid at RH $\lesssim$ 80% (i.e. most of the time during CLACE), and therefore the evaporation rate remains independent from the difference between outdoor and indoor RH. However, the deliquescence relative humidity (DRH) of multicomponent aerosols is considerably lower than that of pure salts (Tang and Munkelwitz, 1993); hence, the Jungfraujoch aerosols are suspected to be in a liquid state even for temperatures well below 0 °C and RH as low as 10% (Fig. 2). This can explain the observed slight (positive) dependence of the particle loss on the difference between outdoor and indoor RH:

$$100(N_{\mathrm{ambient}} - N_{\mathrm{dry}})/N_{\mathrm{ambient}} = 0.4(\mathrm{RH}_{\mathrm{outdoor}}(\%) - \mathrm{RH}_{\mathrm{indoor}}(\%)) + 6.1; \quad R^2 = 0.34.$$

There is no such correlation for the ambient temperature.

Besides ammonium nitrate, volatile organic compounds (VOC) are also expected to be responsible for the observed particle loss. We hypothesize that this loss is partially due to small, newly formed particles that can only be measured at ambient conditions because they evaporate immediately upon entering the warm laboratory.

The particle loss affects almost exclusively the small particles with a dry diameter $D \lesssim 100$ nm. The average loss of particles with dry diameters $D \leq 100$ nm is 35%, whereas the average loss of particles with dry diameters $D > 100$ nm amounts to only 3%. Therefore, though important for the number concentration, the loss has only negligible influences on the surface and volume concentrations. Because there is no close connection between meteorological parameters such as temperature or relative humidity and the amount of particle loss, it is not possible to account for the lost particles by using an empirical model.

The size distributions also show another feature. Some of the spectra surge at a diameter of around 600 nm instead of falling to zero. This property (not very noticeable in the number, but severe in the surface and volume concentration) appears in about 25% of the ambient distributions and 15% of the dry distributions. There is neither a correlation between the surges of dry and ambient spectra nor between surges and particle losses.

3.3. Link between ambient and dry measurements

To link the dry and ambient size distributions, we applied a model based on the following simplifying assumption. The dry aerosol (RH $< 10\%$) consists only of dry material, whereas the ambient aerosol additionally contains a certain amount of water, which is in equilibrium with the (higher) ambient relative humidity. Thus we are confronted with the problem of hygroscopic particle growth as described by the Köhler theory (cf. e.g. Pruppacher and Klett, 1997). To estimate the size of the ambient aerosol, we used the modified Köhler equation introduced by Brechtel and Kreidenweis (2000), which connects the RH to the wet and the dry particle diameter (cf. the Appendix for more details).

A shortcoming of this model is that it does not accommodate phenomena such as hydrophobicity or deliquescence. However, as was mentioned in section 3.1, the hygroscopic growth during the CLACE period was characterized by narrow monomodal growth distributions. The only remarkable deviations from this behavior were two Saharan dust events and local pollution due to construction work. Consequently, data from these time periods were excluded from the analysis presented here.

Figures 5 and 6 show once again the size distributions presented in Figs. 3b and 3c, now complemented by the corresponding corrected dry size distributions

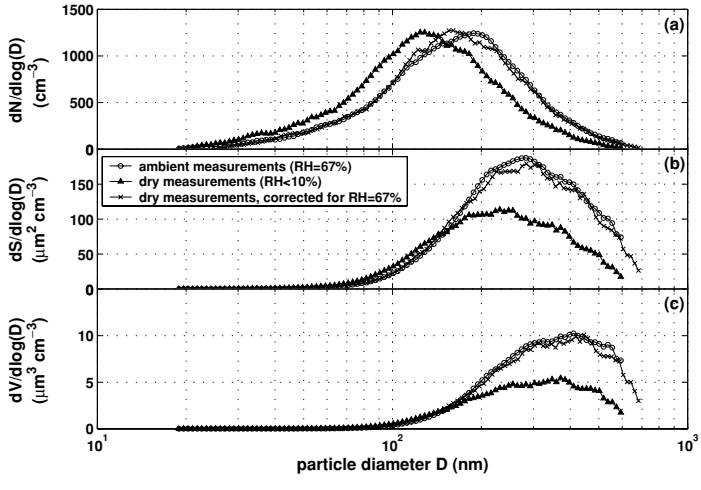

Fig. 5. Ambient, dry and corrected dry size distributions for the same time period (one-hour average) as the number distributions shown in Fig. 3b: (a) number distribution, (b) surface distribution and (c) volume distribution. All distributions are smoothed by 5-bin gliding window averaging.

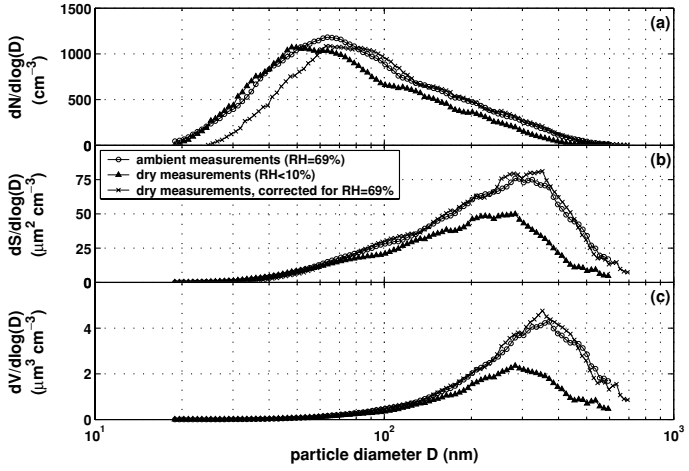

Fig. 6. Ambient, dry and corrected dry size distributions for the same time period (1-h average) as the number distributions shown in Fig. 3c: (a) number distribution, (b) surface distribution and (c) volume distribution. All distributions are smoothed by 5-bin gliding window averaging.

(according to the model described above and in the Appendix). In addition to the number distributions (Figs. 5a and 6a), the corresponding surface (Figs. 5b and 6b) and volume (Figs. 5c and 6c) distributions are given.

For the example in Fig. 5, where the uncorrected dry measurements do not show a reduction in the number concentration, the corrected dry data agree very well with the ambient data for all three distributions. In contrast, as soon as the dry measurements also exhibit a particle loss (e.g. Fig. 6), the ambient number distribution is no longer well represented by the corrected dry number distribution. However, the correction still works well for the surface and volume distributions. This is possible because the particle loss is caused mainly by small particles (see section 3.2 and Fig. 6a), which do not carry great weight in these distributions. Note that only the comparison between the ambient and the corrected dry number distribution in Fig. 6a can show the diameter interval in which the particle loss occurs. Because of the hygroscopic shift, the uncorrected dry distribution misleadingly suggests the particle loss for particles with $D \gtrsim 60$ nm.

In order to evaluate our model for the correction of the dry measurements for the whole CLACE data set, we calculated the following integrated values (for every 1 h average):

$$N_{\mathrm{tot}}^{\mathrm{amb/dry/corr}} := \sum_{i=i_{\min}}^{i_{\max}} n_i^{\mathrm{amb/dry/corr}}\, d\log_i \tag{1a}$$

$$S_{\mathrm{tot}}^{\mathrm{amb/dry/corr}} := \sum_{i=i_{\min}}^{i_{\max}} s_i^{\mathrm{amb/dry/corr}}\, d\log_i \tag{1b}$$

$$V_{\mathrm{tot}}^{\mathrm{amb/dry/corr}} := \sum_{i=i_{\min}}^{i_{\max}} v_i^{\mathrm{amb/dry/corr}}\, d\log_i \tag{1c}$$

where amb, dry and corr denote ambient, dry, and corrected dry measurements. $n_i^{\mathrm{amb/dry/corr}}\, d\log_i$, $s_i^{\mathrm{amb/dry/corr}}\, d\log_i$ and $v_i^{\mathrm{amb/dry/corr}}\, d\log_i$ are the number, surface, and volume concentrations in SMPS channel i, and $d\log_i$ is the logarithmic interval width of channel i.

Here, $i_{\min}$ and $i_{\max}$ were chosen such that the ambient, the dry and the corrected dry concentrations were integrated over the same dry diameter interval (cf. Fig. 4). That is $i_{\min} = D_1$ and $i_{\max} = D_3$ for the (uncorrected) dry distributions, $i_{\min} = D_2$ and $i_{\max} = D_4$ for the wet and the corrected dry distributions. D_1, D_2 and D_3 are defined as described in section 3.2, and D_4 is set to 540 nm in order to avoid result corruption by the surges discussed in section 3.2. A repeated analysis with D_4 set to the upper detection limit of the SMPS systems but excluding all spectra with such surges gave very similar results. Note that D_2 and D_3 depend on ambient RH.

Furthermore, we calculated the following relative deviations of the dry concentrations from the ambient concentrations:

$$\mathrm{dev}_N^{\mathrm{dry}} := \frac{N_{\mathrm{tot}}^{\mathrm{dry}} - N_{\mathrm{tot}}^{\mathrm{amb}}}{N_{\mathrm{tot}}^{\mathrm{amb}}} \quad \text{and} \quad \mathrm{dev}_N^{\mathrm{corr}} := \frac{N_{\mathrm{tot}}^{\mathrm{corr}} - N_{\mathrm{tot}}^{\mathrm{amb}}}{N_{\mathrm{tot}}^{\mathrm{amb}}} \tag{2a}$$

$$\mathrm{dev}_S^{\mathrm{dry}} := \frac{S_{\mathrm{tot}}^{\mathrm{dry}} - S_{\mathrm{tot}}^{\mathrm{amb}}}{S_{\mathrm{tot}}^{\mathrm{amb}}} \quad \text{and} \quad \mathrm{dev}_S^{\mathrm{corr}} := \frac{S_{\mathrm{tot}}^{\mathrm{corr}} - S_{\mathrm{tot}}^{\mathrm{amb}}}{S_{\mathrm{tot}}^{\mathrm{amb}}} \tag{2b}$$

$$\mathrm{dev}_V^{\mathrm{dry}} := \frac{V_{\mathrm{tot}}^{\mathrm{dry}} - V_{\mathrm{tot}}^{\mathrm{amb}}}{V_{\mathrm{tot}}^{\mathrm{amb}}} \quad \text{and} \quad \mathrm{dev}_V^{\mathrm{corr}} := \frac{V_{\mathrm{tot}}^{\mathrm{corr}} - V_{\mathrm{tot}}^{\mathrm{amb}}}{V_{\mathrm{tot}}^{\mathrm{amb}}}. \tag{2c}$$

Table 1 gives mean values of these deviations for several subsets of the CLACE dataset together with the standard deviations of the means. The analysis focuses on time periods without clouds, because only then is the direct aerosol effect important.

The first row of Table 1 reflects the situation for the whole CLACE period when clouds did not affect the station. Without correction the dry measurements considerably underestimate all three concentrations. Note that the underestimation of the number concentration has a different cause than the underestimation of the surface and volume concentration. The first is due to the particle loss discussed in section 3.2, whereas the latter is due to the additional water on the ambient aerosol (hygroscopic behavior). The deficiency cannot be remedied for the number concentration, because our model is not able to compensate for the particle loss, i.e. the corrected and uncorrected total number concentrations are the same. However, the correction leads to substantially more accurate values in the surface and volume concentration, although the volume is slightly overestimated.

Rows 2–4 of Table 1 show the results obtained for cloudless periods divided into different RH regimes. Looking at the surface and volume concentrations, we find that (as expected from the Köhler theory) the differences between ambient and uncorrected dry distributions grow with increasing RH. For RH $< 40\%$ the deviations are still small; however, the corrected dry distributions already reflect the ambient ones better. In the regime $40\% \leq \mathrm{RH} \leq 80\%$ the differences between ambient and uncorrected dry concentrations become substantial, whereas the corrected dry distributions are in good agreement with the ambient ones. However, in the volume concentration the corrected dry values now slightly overestimate the ambient values. This is due to the fact that our model does not account for the possible presence of hydrophobic particles (i.e. particles with $D/D_0 < 1.2$ at RH $= 85\%$). The greater the RH, the greater the importance of the

Table 1. *Relative deviations of the dry from the ambient concentrations as defined in eqs. (2a)–(2c)*

Selected dataset	Number of spectra	Concentration	Uncorrected dry measurements (%)	Corrected dry measurements (%)
Time periods without clouds	476	Volume	-32 ± 1	10 ± 2
		Surface	-29 ± 1	-1 ± 1
		Number	-25 ± 1	-25 ± 1
Time periods without clouds and with RH $< 40\%$	138	Volume	-11 ± 2	3 ± 2
		Surface	-11 ± 2	0 ± 3
		Number	-13 ± 3	-13 ± 3
Time periods without clouds and with $40\% \leq \mathrm{RH} \leq 80\%$	315	Volume	-39 ± 2	12 ± 3
		Surface	-35 ± 1	-2 ± 2
		Number	-30 ± 1	-30 ± 1
Time periods without clouds and with RH $> 80\%$	23	Volume	-64 ± 2	28 ± 8
		Surface	-55 ± 2	7 ± 5
		Number	-33 ± 3	-33 ± 3
Time periods with clouds	95	Volume	-65 ± 3	51 ± 9
		Surface	-57 ± 3	17 ± 5
		Number	-41 ± 2	-41 ± 2
Complete data set (including cloudy periods)	594	Volume	-39 ± 1	17 ± 2
		Surface	-34 ± 1	2 ± 1
		Number	-28 ± 1	-28 ± 1

The table shows mean values and standard deviations of the means for selected datasets as well as the number of spectra contributing to each dataset. The number of spectra of the data sets "time periods without clouds" and "time periods with clouds" do not sum up to the number of spectra of the complete data set, because for some one-hour averages the LWC value, which is necessary for a classification, is missing.

error caused by the presence of such particles, thus explaining why this trend is more pronounced at RH > 80%. However, even for RH > 80% the corrected dry measurements result in a much better match with the ambient measurements than the uncorrected dry measurements.

Although not important for the direct aerosol effect, we also analyzed periods when the JFJ was in clouds since this provides a deeper insight into our hygroscopic model. The cold sampling process eliminates all cloud droplets and leaves only the interstitial aerosol. This means that a major part of the aerosol particles that behave as assumed by our hygroscopic growth model is removed by the 1 μm cut-off of the interstitial inlet because they are activated cloud droplets. This implies that during cloudy periods the sampling technique favors the more hydrophobic particles, which do not behave as the model predicts. Thus, for cloudy periods the corrected dry surface and volume distributions are expected to strongly overestimate the ambient ones. This is indeed the case, as the two last rows of Table 1 show.

4. Conclusions

Simultaneous size distribution measurements were performed at the high alpine research station Jungfraujoch (3580 m asl) under ambient conditions ($T = -10$ °C) and dry indoor conditions ($T = 20$–30 °C). On average, particle number, surface area and volume concentrations under dry indoor conditions were lower by 28%, 34% and 39%, respectively, compared to ambient conditions. We have shown that in the case of surface area and volume concentrations these losses are mainly due to the evaporation of water caused by the decreasing RH in the sampling line. This effect can accurately be corrected by using hygroscopic growth factors. Accurate number concentrations cannot be retrieved, since highly volatile small particles (dry diameter $D \lesssim 100$ nm) are irreversibly lost upon heating from ambient conditions to indoor conditions. Under cloud conditions, the correction was typically too high, because the sampled aerosol in this particular experiment consisted of only the interstitial aerosol particles, which usually exhibit less hygroscopic growth than the particles that are activated into cloud drops. By using an inlet that samples the total aerosol, as is the case for the routine aerosol measurements in the GAW aerosol program (Weingartner et al., 1999), this overestimation of the correction should be minimized. These corrections have important implications, e.g. in the determination of climatically important optical properties of atmospheric aerosol particles (see, e.g. Bundke et al., 2002). These effects will, however, be addressed in a forthcoming paper.

5. Acknowledgments

The financial support and the meteorological data of MeteoSwiss (Global Atmosphere Watch) are highly appreciated. In addition, we thank the International Foundation High Altitude Research Stations Jungfraujoch and Gornergrat (HFSJG), which made it possible for us to carry out our experiments at the High Altitude Research Station at Jungfraujoch. We also thank Martin Gysel, András Hoffer, Matthias Weller and Sebastian Schmidt for assistance in field work and Craig Corrigan and Christina Reynolds for editing the manuscript.

6. Appendix

The modified Köhler equation (A1) (Brechtel and Kreidenweis, 2000) connects the relative humidity, the wet equilibrium and the dry particle diameter:

$$\mathrm{RH} = 100 \exp\left(\frac{4\sigma_\mathrm{w} M_\mathrm{w}}{\rho_\mathrm{w} R T D_\mathrm{wet}}\right) \times \exp\left[\frac{-M_\mathrm{w} c}{1000}\left(Y_f - \frac{A_\Phi c^{1/2} Y_f^{3/2}}{\sqrt{2} + b_\mathrm{pit} c^{1/2} Y_f^{1/2}} + 2c\beta_{0,f} Y_f^2\right)\right], \tag{A1}$$

where c is defined as

$$c \equiv \frac{1000 D_\mathrm{p,sol}^3}{\rho_\mathrm{w}\left(D_\mathrm{wet}^3 - D_\mathrm{p,sol}^3\right)} \tag{A2}$$

and

RH is the relative humidity (%);

σ_w is the surface tension for pure water, $\sigma_\mathrm{w} = 0.077\,65\,\mathrm{N\,m^{-1}}$ at $T = 263.15\,\mathrm{K}$;

M_w is the molecular weight of pure water, $M_\mathrm{w} = 18.0152\,\mathrm{kg\,kmol^{-1}}$;

ρ_w is the density of pure water, $\rho_\mathrm{w} = 998.122\,\mathrm{kg\,m^{-3}}$ at $T = 263.15\,\mathrm{K}$;

R is the universal gas constant, $R = 8314.47\,\mathrm{J\,K^{-1}\,kmol^{-1}}$;

T is the temperature (K);

D_{wet} is the wet particle diameter (m);

$D_{p,sol}$ is the (equivalent) diameter of the soluble fraction of the dry particle (m);

Y_f is a chemical parameter (kmol m^{-3});

A_Φ is the Debye–Hückel coefficient [(kg mol^{-1})$^{1/2}$]

$A_\Phi = 0.1342[0.0368T - 14.6272\ln(T) - 1530.1474T^{-1} + 80.4063]$ for $T < 273$ K (Pitzer, 1991);

b_{pit} is the Pitzer constant, $b_{pit} = 1.2$(kg mol^{-1})$^{1/2}$; and

$\beta_{0,f}$ is a chemical parameter (kg mol^{-1}).

The first term of eq. (A1) represents the Kelvin effect (curvature effect) and the second term Raoult's law (solute effect). This equation was developed for particles completely soluble in water, whereas the aerosols measured during CLACE at the JFJ exhibited a non-soluble volume fraction of 9%–21%, depending on the particle size (Weingartner et al., 2002). This leads to a slightly different use of $D_{p,sol}$: originally simply defined as the dry particle diameter, it denotes in this work the equivalent diameter of the soluble part (79%–91% of the volume, depending on the size of the particles) of the dry particle. However, the difference in the resulting wet diameter is expected to be very small, because the dry particle diameter and the equivalent diameter of the soluble part differ by $\lesssim$5%.

To derive the two unknown chemical parameters Y_f and $\beta_{0,f}$ we used the H-TDMA measurements from 6 March and 16 March 2000 (cf. Fig. 2). For each dry diameter (i.e. 50, 100 and 250 nm) the (D_{wet}, RH) data pairs were fitted (non-linear least squares fit) to the modified Köhler equation (A1).

This procedure yields the values $Y_f = 39 \pm 4$ kmol m^{-3} and $\beta_{0,f} = (-0.1 \pm 0.1) \times 10^{-2}$ kg mol^{-1}, $Y_f = 40 \pm 2$ kmol m^{-3} and $\beta_{0,f} = (-0.5 \pm 0.8) \times 10^{-3}$ kg mol^{-1}, and $Y_f = 41 \pm 5$ kmol m^{-3} and $\beta_{0,f} = (-0.4 \pm 0.6) \times 10^{-3}$ kg mol^{-1} for the dry diameters 50, 100 and 250 nm, respectively (cf. Fig. 2), where the uncertainties were found by a numerical sensitivity study. The fact that Y_f and $\beta_{0,f}$ do not vary within the diameter interval from 50–250 nm implies that the same is true for the chemical composition. Assuming further that the chemical composition is not very different either outside this diameter domain, we used the mean values $\overline{Y_f} = 40$ kmol m^{-3} and $\overline{\beta_{0,f}} = -0.5 \times 10^{-3}$ kg mol^{-1} over the whole diameter interval (18–800 nm) to correct the dry measurements for ambient RH. Even if this assumption were not completely fulfilled, the error in the corrected diameters (wet diameter D_{wet}) would be very small: even an error as big as 200% in $\beta_{0,f}$ causes an error of less than 1% in D_{wet} for RH = 90%. A change of 20% in Y_f leads to a change of 5% in D_{wet} for RH = 90%, whereas for the same deviation in D_{wet} only an error of 2% in RH is tolerated. For smaller RH values the errors in D_{wet} get smaller.

Note that even though we make the simplifying assumption of the same chemical composition over the whole diameter range, this does not imply a constant growth factor over the whole diameter range. Our model takes into account the Kelvin effect, which causes a smaller growth for smaller particles. Hence, the logarithmic channel widths $d\log_i$ are no longer exactly the same after the humidity correction. Although a minor effect, important only for high relative humidity at the lower end of the analyzed particle size range, where the Kelvin effect is most effective, it is considered in the corrected spectra shown in Figs. 5 and 6.

REFERENCES

Brechtel, F. J. and Kreidenweis, S. M. 2000. Predicting particle critical supersaturation from hygroscopic growth measurements in the humidified TDMA. Part I: Theory and sensitivity studies. *J. Atmos. Sci.* **57**, 1854–1871.

Bundke, U., Hänel, G., Horvath, H., Kaller, W., Seidl, S., Wex, H., Wiedensohler, A., Wiegner, H. and Freudenthaler, V. 2002. Aerosol optical properties during the Lindenberg Aerosol Characterization Experiment (LACE 98). *J. Geophys. Res.* **107**, 10.1029/2000JD000188.

Henning, S., Weingartner, E., Schmidt, S., Wendisch, M., Gaeggeler, H. W. and Baltensperger, U. 2002. Size-dependent aerosol activation at the high-alpine site Jungfraujoch (3580 m asl). *Tellus* **54B**, 82–95.

Henning, S., Weingartner, E., Schwikowski, M., Gaeggeler, H. W., Gehrig, R., Hinz, K.-P., Trimborn, A., Spengler, B. and Baltensperger, U. 2003. Seasonal variation of water-soluble ions of the aerosol at the high-alpine site Jungfraujoch (3580 m asl). *J. Geophys. Res.* **108**, 10.1029/2002JD002439.

IPCC. 2001. *Climate Change 2001: The Scientific Basis* (eds. J. T. Houghton, Y. Ding, D. J. Griggs, M. Noguer, P. J. van der Linden, X. Dai, K. Maskell and C. A. Johnson). Cambridge University Press, New York, 881 pp.

Krivacsy, Z., Gelencser, A., Kiss, G., Meszaros, E., Molnar, A., Hoffer, A., Meszaros, T., Sarvari, Z., Temesi, D., Varga, B., Baltensperger, U., Nyeki, S. and Weingartner, E. 2001. Study on the chemical character of water soluble organic compounds in fine atmospheric aerosol at the Jungfraujoch. *J. Atmos. Chem.* **39**, 235–259.

Larson, T. V. and Taylor, G. S. 1983. On the evaporation of ammonium-nitrate aerosol. *Atmos. Environ.* **17**, 2489–2495.

Maenhaut, W., Hillamo, R., Makela, T., Jaffrezo, J. L., Bergin, M. H. and Davidson, C. I. 1996. A new cascade impactor for aerosol sampling with subsequent PIXE analysis. *Nucl. Instr. Meth. (Phys. Res. B)* **109**, 482–487.

Mozurkewich, M. 1993. The dissociation-constant of ammonium-nitrate and its dependence on temperature, relative-humidity and particle-size. *Atmos. Environ.* **27**, 261–270.

Nyeki, S., Baltensperger, U., Colbeck, I., Jost, D. T., Weingartner, E. and Gaggeler, H. W. 1998. The Jungfraujoch high-alpine research station (3454 m) as a background clean continental site for the measurement of aerosol parameters. *J. Geophys. Res.* **103**, 6097–107.

Pitzer, K. S. 1991. *Activity coefficients in electrolyte solutions*. CRC Press, Boca Raton, 542 pp.

Pruppacher, H. R. and Klett, J. D. 1997. *Microphysics of clouds and precipitation*. Kluwer Academic Publisher, Dordrecht, 954 pp.

Ramanathan, V., Crutzen, P. J., Kiehl, J. T. and Rosenfeld, D. 2001. Aerosols, climate, and the hydrological cycle. *Science* **294**, 2119–2124.

Stelson, A. W. and Seinfeld, J. H. 1982. Relative humidity and temperature dependence of the ammonium nitrate dissociation constant. *Atmos. Environ.* **16**, 983–992.

Tang, I. N. and Munkelwitz, H. R. 1993. Composition and temperature-dependence of the deliquescence properties of hygroscopic aerosols. *Atmos. Environ.* **27**, 467–473.

Tenberken-Pötzsch, B., Schwikowski, M. and Gäggeler, H. W. 2000. A method to sample and separate ice crystals and supercooled cloud droplets in mixed phased clouds for subsequent chemical analysis. *Atmos. Environ.* **34**, 3629–3633.

Weingartner, E., Nyeki, S. and Baltensperger, U. 1999. Seasonal and diurnal variation of aerosol size distributions ($10 < D < 750$ nm) at a high-alpine site (Jungfraujoch 3580 m asl). *J. Geophys. Res.* **104**, 26809–26820.

Weingartner, E., Gysel, M. and Baltensperger, U. 2002. Hygroscopicity of aerosol particles at low temperatures. 1. New low-temperature H-TDMA instrument: setup and first applications. *Environ. Sci. Technol.* **36**, 55–62.

WMO. 2001. *Strategy for the implementation of the Global Atmosphere Watch Programme (2002–2007)*, WMO No. 142. World Meteorological Organization, Geneva, Switzerland.